The following publication Hsu, L. T., Tokura, H., Kubo, N., Gu, Y., & Kamijo, S. (2017). Multiple Faulty GNSS Measurement Exclusion Based on Consistency Check in Urban Canyons. IEEE Sensors Journal, 17(6), 1909-1917 is available at http://dx.doi.org/10.1109/JSEN.2017.2654359

Multiple Faulty GNSS Measurement Exclusion based on Consistency Check in Urban Canyons

Li-Ta Hsu, *Member,* Hiroko Tokura*, non-Member,* Nobuaki Kubo*, Member, IEEE*, Yanlei Gu, *Member, IEEE*, and Shunsuke Kamijo, *Member, IEEE*

***Abstract*— Sensors play important roles for autonomous driving. Localization is definitely a key one. Undoubtedly, global positioning system (GPS) sensor will provide absolute localization for almost all the future land vehicles. In terms of driverless car, 1.5 meters of positioning accuracy is the minimum requirement since the vehicle has to keep in a driving lane that usually wider than 3 meters. However, the skyscrapers in highly-urbanized cities such as Tokyo and Hong Kong, dramatically deteriorate GPS localization performance, leading more than 50 meters of error. GPS signals are reflected at modern glassy buildings which caused the notorious *multipath* effect. Fortunately, the number of navigation satellite is rapidly increasing in a global scale since the rise of multi-GNSS (global navigation satellite system). It provides an excellent opportunity for positioning algorithm developer of GPS sensor. More satellites in the sky implies more measurements to be received. Novelty, this paper proposes to take advantage of the fact that clean measurements (refers to line-of-sight measurement) are consistent and multipath measurements are inconsistent. Based on this consistency check, the faulty measurements can be detected and excluded to obtain better localization accuracy. Experimental results indicate that the proposed method can achieve less than 1 meter lateral positioning error in middle urban canyons.**

***Index Terms*— GPS; GNSS; Multipath; Localization; Navigation; Autonomous Driving; Urban Canyon; Land Application**

I. Introduction

Autonomous driving requires accurate locating service provided by sensors in all environments [1, 2]. Global positioning system (GPS) sensor provides absolute localization service in all outdoor areas in all weather conditions [3]. In open-sky areas, GPS sensor can achieve up to sub-meter positioning accuracy if differential correction is available [4, 5]. However, particularly in Asian highly-urbanized city, dense skyscrapers and narrow streets strongly challenge the GPS localization performance in two aspects, blockage and reflection [6]. The number of GPS satellite, which its elevation higher than 10 degrees and not blocked by obstacles, is very limited in the challenging environments. Urban canyons typically block many line-of-sight (LOS) signals. Fortunately, with the rise of multi-GNSS (global navigation satellite system), the navigation signal availability in urban environments has been greatly enhanced, making it easy to receive American GPS, Russian GLONASS, Chinese Beidou, and Japanese QZSS signals at the same time [7]. The number of visible satellites in such environments could now be between 15 and 30, especially for Asia Pacific region [8]. However, at meanwhile, it also increases the number of *multipath*-effected signals. Thus, GNSS performance in highly urbanized area can still be deteriorated to about 50 meters [9].

There are several approaches to deal with the *multipath* effects. Conventionally, GPS sensor manufacturer designs special correlator, leading sharper correlation shape to mitigate multipath effect. [10-12]. It is effective in dealing with middle or long range multipath, but not in reducing the short one, which could still induce a few tens of meter in pseudorange error. In addition, this conventional technique offers little improvement on non-line-of-sight (NLOS) reception. Approaches to NLOS mitigation are therefore needed. Novel receiver-based technique, vector tracking, is proposed to utilize the dynamic model of receiver to predict the code/carrier frequencies [13]. This characteristic can detect both multipath and NLOS signals to further mitigate their effect of localization accuracy [14]. Even through the main benefit of vector tracking is information exchange among the channels, but this sharing procedure could be the source of a new problem for the receiver [15]. This new problem of vector tracking is that tracking error in a channel can potentially influence other channels and resulting in degradation in the positioning accuracy.

Recently, sensor integration became a major research stream. To compensate the effect of GPS outage caused by multipath and NLOS, GPS integrates with other sensors or additional information such as low-cost MEMS level inertial navigation system (INS) [16-21], magnetometer and other sensors [22, 23] and 3D digital maps [24-26]. This paper aims to enhance GPS performance before its integration with other sensors. The inspiration is that the opportunity provided by existing multi-GNSS enables the number of LOS GNSS (visible) satellites is more than 10 even in the case of urban canyons [8]. It is possible to use only LOS satellites in these problematic environments, however, it is difficult to distinguish the signal type, namely LOS, NLOS and multipath, without the help of 3D building models [27, 28] or camera attached on the top of vehicle [29, 30].

A potential solution is to apply consistency check, which is based on multipath/NLOS contaminated measurement is not consist with other clean measurements [31]. The fault detection

L.T. Hsu, is with Hong Kong Polytechnic University, Hong Kong (e-mail: lt.hsu@polyu.edu.hk). H. Tokura and N. Kubo are with Tokyo University of Marine Science and Technology, Japan (lacto.h@gmail.com; nkubo@kaiyodai.ac.jp) Y. Gu and S. Kamijo are with the University of Tokyo, Japan (e-mail: guyanlei@kmj.iis.u-tokyo.ac.jp; kamijo@ iis.u-tokyo.ac.jp).

using the idea consistency-checking is able to detect the multipath effects. Famous receiver autonomous integrity monitoring adopts the same working principle to calculate the integrity for GPS receiver [32-34]. Toyota ITS team also releases a report to show the effeteness of consistency check to exclude multipath range error for vehicle application [35]. In 2015, a simulation result of multiple fault detection and exclusion (FDE) with large number of pseudorange measurements is released to show its capability in the area that high probability of measurement fault [36]. The objective of this study is to develop practical multiple FDE algorithms based on consistency check and evaluate them in real urban environments in terms of localization accuracy.

This paper uses measurements of GPS, GLONASS, Beidou, and QZSS collected by land vehicle. Marunouchi, close to Tokyo train station, a metropolitan highway, and Ginza are selected as the study areas due to their density of buildings and skyscrapers. The research team of Tokyo University of Marine Science and Technology has previously shown the effectiveness of the signal quality constraints and the differential GNSS (DGNSS) system in urban environments [37]. This study extends this previous work and implements the consistency check based multiple FDE algorithm. With the aid of DGNSS, the offset between different constellation systems can be cancelled. Thus, all the GNSS measurements are synchronized, which improves the consistency check algorithm. Two FDEs are proposed: greedy and exhaustive FDEs. The greedy search FDE excludes the biased satellites one by one until the test statistic satisfies the chi-squared threshold. It is a computationally effective algorithm that can be implemented in real-time. The exhaustive FDE tests all the possible subset of satellites to find the most consistent group of satellites, which can be regarded as the theoretically optimal result in terms of the consistency check. Although its computational load is excessive, it can be used to understand the limitation of single frequency pseudorange level positioning.

In Section II of this paper, we introduce the consistency check based fault detection algorithm. The developed greedy and exhaustive FDEs are introduced in Section III. Experiment setup and results are shown in Section IV. Finally, conclusions and implications of this study are summarized in Section V.

II. Fault Detection Based on Consistency Check

The geometric relationship between receiver position and satellite position can be linked by the pseudorange measurement. The linearized equation can be expressed as:

$$\boldsymbol{\rho} = \boldsymbol{G}\boldsymbol{x} + \boldsymbol{\varepsilon} \tag{1}$$

where $\boldsymbol{\rho}$ denotes the pseudorange measurement, $\boldsymbol{G}$ denotes the observation matrix, which consists of the unit LOS vector between the satellite and assumed receiver position, and $\boldsymbol{x}$ is the receiver states, shown in (2). $\boldsymbol{\varepsilon}$ is an error term and shown in (3).

$$\boldsymbol{x} = \begin{bmatrix} x & y & z & b_{rcv,clk} \end{bmatrix}^T \tag{2}$$

$$\boldsymbol{\varepsilon} \in N(0, \boldsymbol{W}^{-1}) \tag{3}$$

The receiver state is defined as the receiver position in three directions and the receiver clock bias relative to GPS system time. The error is assumed to be Gaussian with zero mean and a known covariance. The covariance is usually calculated by the inverse of a weighting matrix $\boldsymbol{W}$. The error of each satellite is assumed to be independent of each other. With the weighted least squares (WLS) estimation, the receiver states can be estimated using (4).

$$\hat{\boldsymbol{x}} = (\boldsymbol{G}^{\boldsymbol{T}}\boldsymbol{W}\boldsymbol{G})^{-1}\boldsymbol{G}^{\boldsymbol{T}}\boldsymbol{W}\boldsymbol{\rho} = \boldsymbol{K}\boldsymbol{\rho} \tag{4}$$

The $\boldsymbol{K}$ matrix is the weighted pseudo-inverse of the $\boldsymbol{G}$ matrix. The consistency between measurements can be judged by the pseudorange residual as:

$$\hat{\boldsymbol{\varepsilon}} = \boldsymbol{\rho} - \boldsymbol{G} \cdot \hat{\boldsymbol{x}} \tag{5}$$

If an enormous error is contained in one of the pseudorange measurements, it will affect the goodness of the least squares fit because of the inconsistency with other, clean pseudorange measurements. The weighted sum of the square error (WSSE) is calculated and used as a test statistic to indicate the goodness of the least squares fit. The WSSE can be calculated by [34]:

$$WSSE = \hat{\boldsymbol{\varepsilon}}^{\boldsymbol{T}}\boldsymbol{W}\hat{\boldsymbol{\varepsilon}} \tag{6}$$

The pseudorange residual is assumed as a normally distributed zero mean random variable if all the measurements are clean. Thus, the *WSSE* can be tested by the chi-square test using an appropriate degree of freedom (DOF) and probability of false alarm (P_{FA}). The threshold of the chi-square test can be calculated as the equations below [34]:

$$1 - P_{FA} = \frac{1}{\Gamma(DOF/2)} \int_0^{CT^2} e^{-s} s^{\frac{DOF}{2}} ds \tag{7}$$

$$DOF = N_{SV} - N_{state} \tag{8}$$

where CT is the threshold value of the chi-square test, N_{SV} denotes the number of satellites in the new subset of satellites, and N_{state} denotes the number of unknowns in the state. If multipath-effected measurement presented in measurements, there is $1 - P_{FA}$ of probability that the measurements cannot pass the chi-squared test. To conduct the fault detection, at least one DOF is required, i.e. $DOF \geq 1$,. If the test statistic is smaller than the threshold, the solution is valid. On the contrary, if the *WSSE* is larger than the threshold, a fault exclusion technique is required. In the estimation theory, the calculation of the *WSSE* is based on the L_2 norm minimization. L_2 norm minimization is able to give a stable and non-sparse solution with efficient computational load [38, 39]. The purpose of the consistency-check is to find a group of good quality

measurements, namely a self-consistent group (the sparsest solution).

In implementation of the fault detection, an iterative WLS is used to obtain the receiver states. The initial guess of the receiver state is $\boldsymbol{x_0}$, and the state is defined as the correction to the receiver position and clock bias. (9) shows the estimated state in the iterative WLS.

$$\boldsymbol{\delta\hat{x}} = (\boldsymbol{G^T W G})^{-1}\boldsymbol{G^T W \delta\rho} = \boldsymbol{K\delta\rho} \tag{9}$$

This paper applies a C/N_0-based weighting method [40]:

$$W^{(k)} = \sqrt{const \cdot 10^{-C/N_0{}^{(k)}/10}} \tag{10}$$

where C/N_0 is the carrier noise ratio measured by the receiver and $const = 1.1\times10^4$ is a constant [40]. In urban areas, the C/N_0 based weighting method is more appropriate than the elevation based weighting method because the NLOS reception usually has a weak C/N_0 but enters at a relatively high elevation angle [27]. After obtaining $\boldsymbol{\delta\hat{x}}$, the receiver state can be updated by $\boldsymbol{\hat{x}} = \boldsymbol{x_0} + \boldsymbol{\delta\hat{x}}$. The iteration stops if the position is converged, i.e. $\|\boldsymbol{\delta\hat{x}}\| < 10^{-7}$ in this study. The pseudorange residual can be calculated using the estimated receiver state by iterative WLS, as shown in (11).

$$\hat{\varepsilon}^{(k)} = \rho_c^{(k)} - \hat{r}^{(k)} \tag{11}$$

$$\rho_c^{(k)} = \rho^{(k)} - \hat{b}_{rcv,clk} - \delta\rho_{DGNSS}^{(k)} \tag{12}$$

$$\hat{r}^{(k)} = \sqrt{\left(x_{sv}^{(k)} - \hat{x}\right)^2 + \left(y_{sv}^{(k)} - \hat{y}\right)^2 + \left(z_{sv}^{(k)} - \hat{z}\right)^2} \tag{13}$$

where $\rho_c^{(k)}$ denotes the corrected pseudorange from the k^{th} satellite and can be expressed by (12). The raw pseudorange measurement collected from the receiver, ρ, is biased. We apply the DGNSS correction to eliminate the ionospheric, tropospheric, and satellite orbit and clock error for GNSS pseudorange measurements. For GLONASS or Beidou measurements, the system time offset between the GPS and the other constellations is also provided in the DGNSS correction $\delta\rho_{DGNSS}^{(k)}$. Therefore, all the corrected GNSS pseudorange measurements are synchronised to GPS system time. In addition, the estimated receiver clock offset is also used to correct the pseudorange. $\hat{r}^{(k)}$ denotes the geometric distance between the k^{th} satellite to the estimated receiver position. The geometric distance $\hat{r}^{(k)}$ is calculated by (13). Then, we substitute (11) into (6) to obtain the *WSSE*. To reduce the computational load, the value of the chi-square threshold is calculated in advance and used as constant value. In this study, the number of states is 4, therefore, we need at least 5 satellites to conduct the consistency check based fault detection. This single fault assumption may not be true in urban environments. However, based on the consistency check, the LOS measurements are consistent and the multipath measurements are inconsistent. Ideally, the number of LOS measurements should be more than that of multipath or NLOS effected measurements. Thus, based on this consistency check, the faulty measurements can be detected and excluded to obtain better accuracy.

III. Multiple Faults Exclusion

After detected the existence of faulty measurements, the exclusion of it has to be conducted. There are two FDE methods developed, exhaustive and greedy searches. The former and latter ones represent the theoretically and practical performance of the consistency-check based FDE, respectively.

A. Exhaustive Search

If the test statistic calculated by all satellites in view cannot pass the chi-square test, one or several satellites should be excluded to find a group of healthy measurements. Ideally, we should test all the possible group of satellites, namely all subsets, to find the most consistent one. The subset with all satellites in view, SV^{all}, can be expressed as:

$$\boldsymbol{SV^{all}} = \{1, \ldots, N_{SV}\} \tag{14}$$

The subsets of excluded satellites, $\boldsymbol{SV^{ex}}$, are expressed as:

$$\forall \boldsymbol{SV^{ex}} \begin{cases} \boldsymbol{SV^{ex}} \subset \boldsymbol{SV^{all}} \\ dof(\boldsymbol{SV^{ex}}) \geq 2 \end{cases} \tag{15}$$

$$\text{where } dof(\boldsymbol{SV^{ex}}) = \left|\boldsymbol{SV^{all}}\right| - \left|\boldsymbol{SV^{ex}}\right| - N_{state} \tag{16}$$

where $|SV^{ex}|$ denotes the number of elements in the subset SV^{ex}. (15) shows that $\boldsymbol{SV^{ex}}$ is a subset of $\boldsymbol{SV^{all}}$. In the exclusion of a single satellite fault, the number of DOF should be at least two, i.e., $DOF \geq 2$. This is because the fault exclusion requires a second layer of consistency-check based fault detection to verify that the new subset, after exclusion, is fault-free. Fig. 1 shows the flowchart of the multiple FDE used.

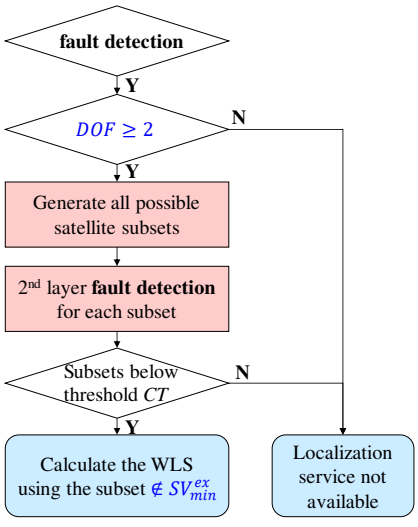

Fig. 1. Flowchart of the multiple FDE based on the exhaustive search.

The second layer of fault detection is the same as the fault detection mentioned in Section II. After the 2nd fault detection we can determine the subsets that passed the fault detection. If

there are multiple subsets that passed the chi-square test, the subset with the largest number of measurements is selected, as shown in (17):

$$\boldsymbol{SV}^{\boldsymbol{ex}}_{\max \boldsymbol{N_{SV}}} = \arg\max_{i}\{|SV^{ex}(i)||WSSE(\boldsymbol{SV}^{\boldsymbol{ex}}) < CT(DOF, P_{FA})\} \quad (17)$$

where i denotes the index of subset SV^{ex}. If there are multiple subsets with an identical number of measurements, namely $\left|SV^{ex}_{\max N_{SV}}\right| > 1$, the subset with the minimum test statistic is selected. As indicated in Appendix F in [41], the minimized chi-square test statistic is a good choice for exclusion, thus, we can identify the satellites that should be excluded using equation (18).

$$SV^{ex}_{min} = \arg\min_{j}\left\{WSSE\left(\boldsymbol{SV}^{\boldsymbol{ex}}_{\max \boldsymbol{N_{SV}}}(j)\right)\right\} \quad (18)$$

where j denotes the index of subset $SV^{ex}_{\max N_{SV}}$. Ideally, the most consistent solution can be found by finding the minimum test statistic in all the possible subsets of satellites. However, the computational load will be extremely high in the multi-GNSS scenario. For example, the number of all the subsets in the case of 20 satellites in view is the sum of the binomial coefficients from using 6 to 20 satellites, namely $C_{20}^{20} + C_{19}^{20} + \cdots + C_{6}^{20}$. This is not practical for real-time application but it can provide a baseline to evaluate the practical fault exclusion algorithms.

B. *Greedy Search*

For the sake of fast calculation, we apply a greedy search fault exclusion method. The greedy algorithm is used to find the local optimal choice at each loop or stage. In other words, we assume that only one satellite is contaminated at a time. Although this assumption is not always true in urban environments, simulation results indicate that the greedy search algorithm shows similar performance to the exhaustive search if only a small number of satellite faults exist. The simulation assumes all faults have a similar probability of occurring and are uncorrelated with each other, which is a valid assumption in city environments. The main characteristic of the greedy search based fault exclusion is to exclude the inconsistent measurements one by one. The flowchart of the greedy search based FDE is shown in Fig. 2. Firstly, if the test statistic calculated by all the satellites in view cannot pass the chi-square test, we generate subsets excluding only one satellite from the group of survived satellites, $\boldsymbol{SV}^{\boldsymbol{survived}}$, as shown in (19).

$$\forall \boldsymbol{SV}^{\boldsymbol{ex}} \begin{cases} \boldsymbol{SV}^{\boldsymbol{ex}} \subset \boldsymbol{SV}^{\boldsymbol{survived}} \\ DOF(\boldsymbol{SV}^{\boldsymbol{ex}}) \geq 2 \\ |\boldsymbol{SV}^{\boldsymbol{ex}}| = 1 \end{cases} \quad (19)$$

$\boldsymbol{SV}^{\boldsymbol{survived}}$ is initialized by $\boldsymbol{SV}^{\boldsymbol{all}}$. Note that the number of element in the subsets $\boldsymbol{SV}^{\boldsymbol{ex}}$ in the greedy exclusion is always 1. If several subsets pass the 2nd fault detection, then the subset with the minimum test statistic is selected, as mentioned in (17) and (18). If none of the subsets pass the check, we exclude $SV^{ex}_{min} = \arg\min_{i}\{WSSE(\boldsymbol{SV}^{\boldsymbol{ex}}(i))\}$ from the $\boldsymbol{SV}^{\boldsymbol{survived}}$. The iteration will stop until the remaining set of the measurements is self-consistent or the DOF is insufficient.

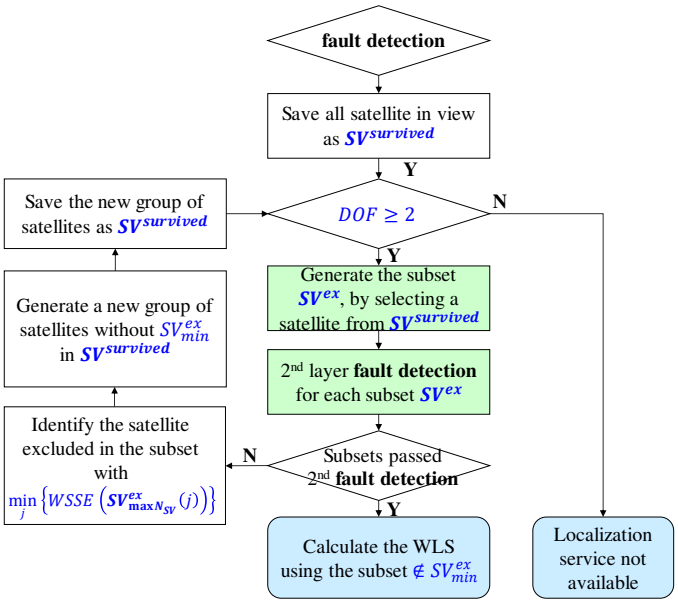

Fig. 2. Flowchart of the multiple FDE based on the greedy search.

IV. Experimental Results and Discussions

A. *Experiment setup*

This study used the raw experimental GNSS data and ground truth data provided by the SIP-adus project. SIP-adus stands for strategic innovation promotion program of automated driving systems. It is initiated by cabinet office, government of Japan, to accelerate the development on automated driving. GNSS antenna and receiver were set up in a moving vehicle as a rover. The reference station for differential GNSS was set within 4 kilometres of the vehicle path. Regarding the ground truth, the positioning solutions calculated by mobile mapping system were used. The rover, the reference station, Trimble multi-GNSS receivers (SPS855 and NetR9, respectively), and Trimble multi-GNSS antennas were used. Satellite constellations included GPS, GLONASS, BeiDou, and QZSS. Rover moving tests were performed in a city urban environment in Tokyo, Japan, on the 13th and 14th of December 2014 and L1 raw data were obtained at approximately 66 and 48 minutes, respectively, at a frequency of 5 Hz. The experimental routes are shown in Fig. 3. The vehicle drove through all typical environments in Tokyo city, including open-sky, middle canyons, and deep urban canyons. The following three methods were compared:

1). DGNSS using all satellites in view,
2). DGNSS + FDE based on a greedy search, and
3). DGNSS + FDE based on an exhaustive search (theoretical best result).

Fig. 3. Study areas, including open-sky, sub-urban, middle-urban, and deep urban environments. The yellow line indicates the driving route. Photo credits: Google Earth.

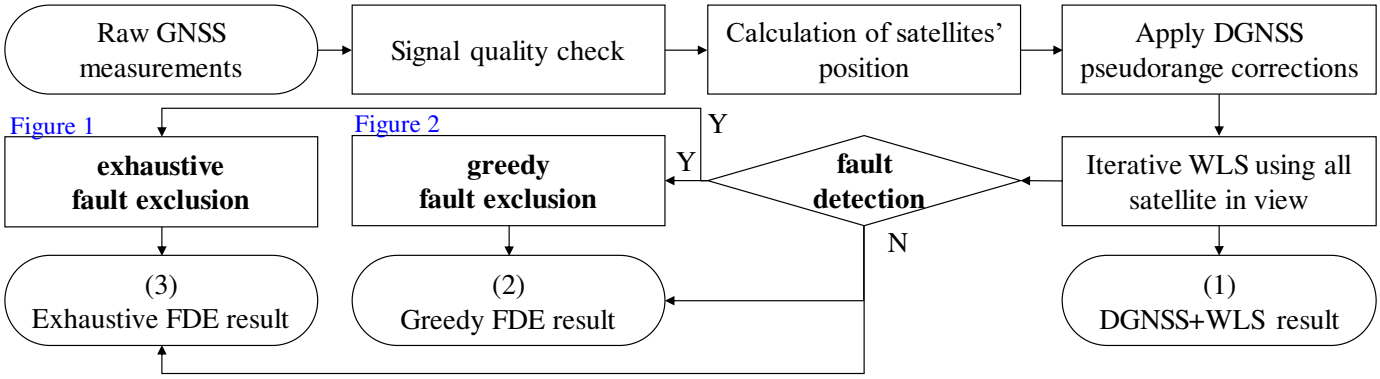

Fig. 4. Flowchart of the testbed.

Fig. 4 shows the flowchart of the testbed. The detailed signal quality check and generation of the DGNSS correction can be found in [37]. We evaluated performance based on the lateral positioning error. The results shown in this paper are single point positioning, in other words, results are independent between different epochs of data.

B. All Environments

The experimental results of the multiple FDE based on the greedy search are shown in Fig. 5. The green points indicate the results that passed the consistency check without excluding any satellites, i.e., they are identical to the results of DGNSS using all satellites. The red points indicate the results that passed the consistency check after excluding faulty satellites. The blue points indicate the results that did not pass the consistency check due to an insufficient number of healthy measurements. In the top panels of Fig. 5, the lateral errors of the red points are lower than that of the green and blue points in most cases. The middle panel shows that exclusion of one or two satellites is sufficient to find a self-consistent group of satellites, especially in open-sky areas. Note that a few red points in the middle and urban canyon environments have larger positioning errors than the green points. The reason for this will be discussed in the next subsection.

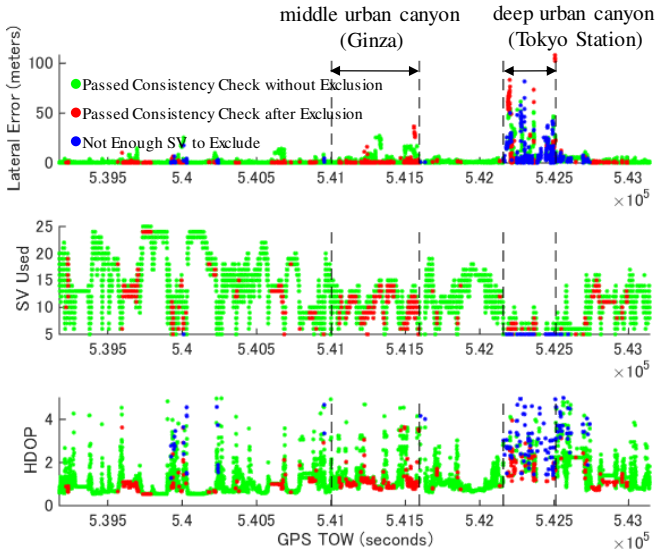

Fig. 5. Experimental results of 1213 using the multiple FDE based on the greedy search

TABLE I shows the performance comparison using the three methods. DGNSS can achieve 1.45 metres of mean error. By applying the consistency check based on the greedy search, the mean error can be reduced to 1.03 metres. However, the

availability is lost little if FDEs are applied. The performance of the FDE based on the greedy search is very similar to that based on the exhaustive search, in terms of the mean error. The percentage of all solutions with less than 1.5 metres of error increases by approximately 5.0 % with the aid of FDEs. With respect to the results with a large positioning error, both FDEs can reduce the error by approximately 1.4 %. FDE can greatly facilitate the performance of the DGNSS, making it suitable for use in autonomous driving applications. For these applications, middle and urban canyons are the most challenging environments. The next subsections are focused on the evaluation of middle and deep urban areas.

TABLE I
PERFORMANCE OF THE THREE METHODS USING ALL DATA

All data (19840+14230 epochs)	DGNSS	DGNSS Greedy FDE	DGNSS Exhaustive FDE
Mean error	1.45 m	1.03 m	0.99 m
Maximum error	81.72 m	108.2 m	108.2 m
Percentage (<1.5 metres)	77.33 %	82.43 %	82.31 %
Percentage (<3.0 metres)	84.03 %	87.59 %	87.58 %
Percentage (>10.0 metres)	1.98 %	0.77 %	0.60 %
Availability	92.57 %	91.84 %	91.98 %

C. *Middle Urban Canyon*

TABLE II shows the performance of the three methods in middle urban canyons.

TABLE II
PERFORMANCE OF THE THREE METHODS IN THE MIDDLE URBAN CANYON.

All data (2954+2505 epochs)	DGNSS	DGNSS Greedy FDE	DGNSS Exhaustive FDE
Mean error	1.75 m	0.76 m	0.67 m
Maximum error	27.25 m	36.52 m	13.95 m
Percentage (<1.5 metres)	70.90 %	87.67 %	87.07 %
Percentage (<3.0 metres)	80.40 %	93.50 %	93.26 %
Percentage (>10.0 metres)	2.11 %	0.46 %	0.11 %
Availability	95.38 %	95.38 %	95.38 %

Firstly, no points in the middle urban canyons lack healthy measurements, thus the availability of DGNSS and DGNSS + consistency check are the same. In the middle urban canyon, the DGNSS can achieve 1.75 metres of mean error. Approximately 2.1 % of the results have a large positioning error. With the aid of the greedy FDE, the percentage of the large error is reduced to less than 0.5 %. This result indicates that the consistency check algorithm is very useful for DGNSS positioning in middle urban canyons because of the sufficiency of healthy measurements. For application to autonomous driving, it is important to obtain a performance where the lateral error is smaller than half a lane width, namely less than 1.5 metres. The greedy FDE method results in more than 87.6 % of measurements with this performance in middle urban canyons. Performances of the greedy and exhaustive searches are very similar, except for the maximum error. Fig. 6 shows plots of the positioning error of the DGNSS method and the two FDE methods. The consistency-check based FDEs are able to reduce the jumping error. To compare the red points and blue circles in Fig. 6, a few of the greedy search points clearly show a large positioning error for both middle urban canyons. We select the Ginza case (top panel in Fig. 6) to discuss the difference between the two FDE methods.

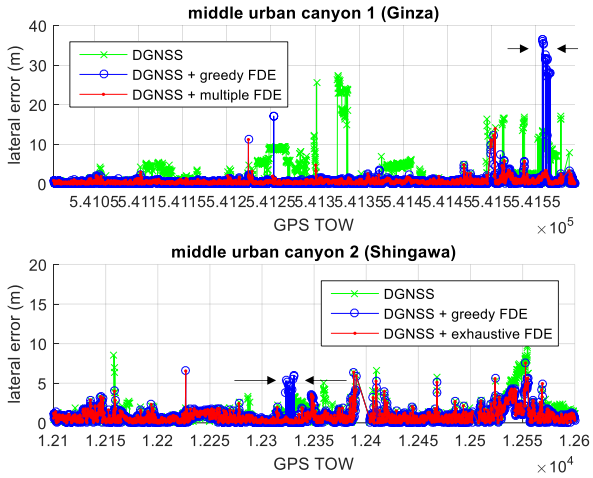

Fig. 6. Lateral positioning error of the greedy and exhaustive searches in middle urban canyons.

As shown in the grey box in Fig. 7, the error of the blue circles is larger than that of the green crosses.

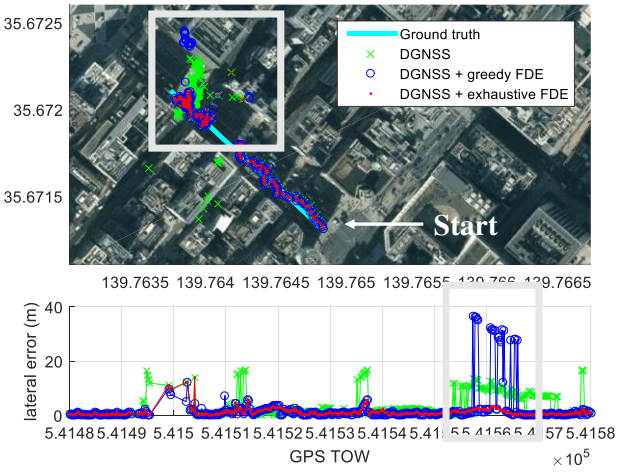

Fig. 7. Positioning results in the period that the exhaustive search outperformed the greedy search.

This implies that the greedy search excludes a healthy measurement instead of an erroneous one. The error of the red points is smaller than that of the green circles, which indicates that the exhaustive search excludes the faulty satellites successfully. Fig. 8 is a rough skyplot that shows that the greedy search first excludes R10 and then G05. For the exhaustive search, the first satellite excluded is also R10 in the case of one satellite exclusion. However, in the case of two satellite exclusions, the exhaustive search excludes R23 and

C07. As can be seen from Fig. 8, the greedy search excludes two satellites with higher elevation angle. This result shows that, in some cases, the greedy FDE is not capable of finding the most self-consistent group of healthy measurements.

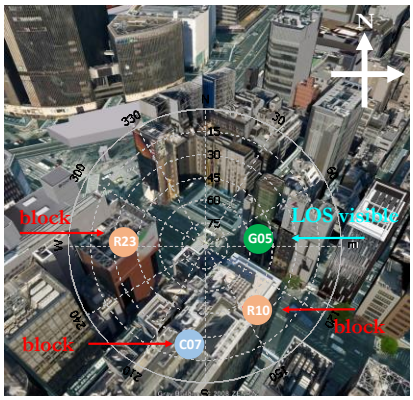

Fig. 8. Skyplot showing the case where the greedy search excludes the wrong satellites. Photo credit: Google Earth.

D. Deep Urban Canyon

Fig. 9 shows the positioning results of the three methods for deep urban canyons. The bottom panel of the Fig 9. shows that the number of received satellites was less than 10 in the majority of cases, which resulted in poor satellite geometries. TABLE III shows the performance of the three methods in the deep urban canyon environment.

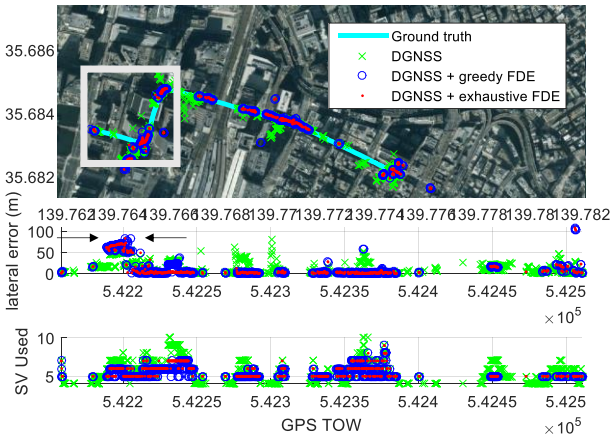

Fig. 9. Positioning results in the period that exhaustive search outperformed greedy search.

TABLE III
PERFORMANCE OF THE THREE METHODS IN THE DEEP URBAN CANYON.

All data (1766 epochs)	**DGNSS**	**DGNSS Greedy FDE**	**DGNSS Exhaustive FDE**
Mean error	12.17 m	12.78 m	11.18 m
Maximum error	81.72 m	108.18 m	108.18 m
Percentage (<1.5 metres)	10.73 %	10.06 %	10.73 %
Percentage (<3.0 metres)	24.86 %	20.73 %	22.66 %
Percentage (>10.0 metres)	24.80 %	10.23 %	8.14 %
Availability	64.04 %	38.08 %	39.38 %

As shown in TABLE III, DGNSS alone has only approximately 64 % availability, therefore, for 36 % of the time, the rover receiver cannot receive more than 4 satellites. The mean error of the DGNSS alone is 12.17 metres. The greedy FDE provides very limited assistance in this environment. Compared to the greedy search, the exhaustive search can reduce the mean error by almost 1 metre. In terms of availability of the two FDE algorithms, the greedy and exhaustive search can only provide about 38.08 % and 39.38 %, respectively. Both FDEs are less capable of finding the sparsest solution in the case of insufficient healthy measurements. In order to investigate the problems that both FDEs have in deep urban canyon, we analyse the area in the grey box in Fig. 9. Firstly, we manually construct basic 3D building models in the area of Tokyo station, as shown in Fig. 10, and then use them to generate the skyplot shown in Fig. 11.

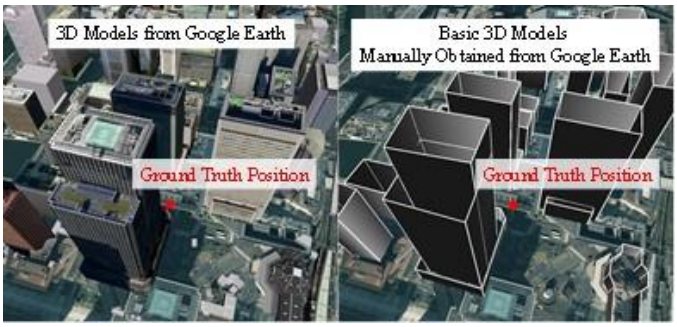

Fig. 10. Basic 3D building models constructed from Google Earth.

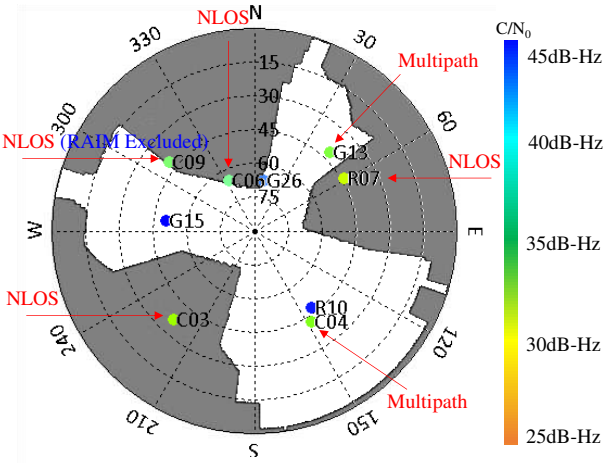

Fig. 11. Skyplot of satellites received in the area of the grey box in Fig. 10. G, R and C indicate GPS, GLONASS and Beidou satellites, respectively.

The grey colour denotes blockage by the buildings generated from Fig. 10. The colour of satellites denotes the received signal strength. In the selected area, there are 9 satellites received, including 3 LOS, 2 multipath, and 4 NLOS signals. Both FDE methods find the most consistent group of satellites after excluding C09. However, there are still 3 NLOS and 2 multipath signals left. The consistency check method therefore finds the most consistent but erroneous group of satellites. This

erroneous group of satellites results in a large faulty positioning solution.

E. Discussion

The classified positioning results based on the number of received satellites are shown in Fig. 12(a). Fig. 12(b) shows the number of epochs for different numbers of satellites. TABLE IV shows the environment definitions based on the number of received satellites. Fig. 12(a) suggests that the FDE methods show little improvement in open-sky scenarios. In middle urban canyons, both FDE methods can greatly reduce the positioning error, moreover, the performance of the greedy search is almost the same as that of the exhaustive search. Where less than 10 satellites are received, the greedy search is less capable of finding the sparsest solution. In the case where a very limited number of satellites are received, i.e. 6, the consistency check method cannot exclude all the erroneous satellites due to the lack of healthy measurements.

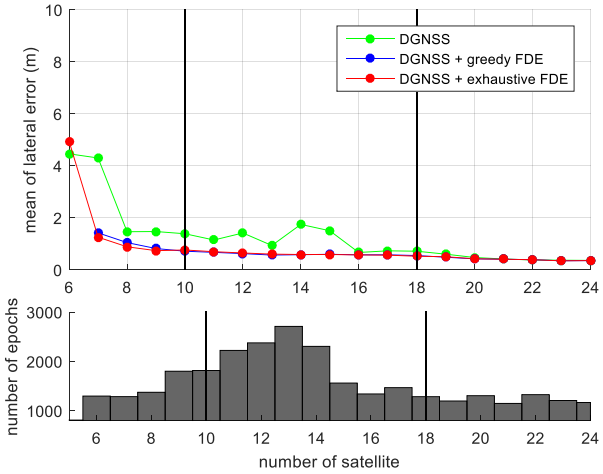

Fig. 12 (a) Mean lateral error of the proposed methods based on number of received satellites. (b) Number of epochs based on number of received satellites.

TABLE IV
DEFINITION OF SCENARIOS BASED ON NUMBER OF RECEIVED SATELLITES

Scenarios	*Open sky*	*Middle urban*	*Deep urban*
number of SV	>18	18-10	<10

The low-cost sensor is more favourable for majority of applications. Additional testing drives are also performed in Tokyo city to collect data from a low-cost receiver, u-blox M8. The area also contains many scenarios, including open-sky area, middle-class urban and deep urban canyons. The commercial receiver used currently cannot acquire Beidou and GLONASS simultaneously. Thus, its number of received satellite is less comparing with the geodetic receiver. Fig. 13 shows its result. As can be seen, the performance of using GNSS receiver with the proposed consistency check methods commercial is similar to using geodetic receiver. The proposed methods also improve the most when number of received satellite in between 10 to 15. In the other words, the proposed methods are effective for both geodetic and consumer level GNSS sensors.

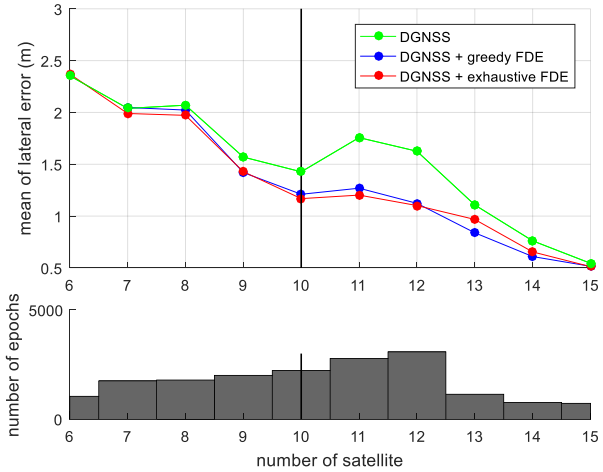

Fig. 13. (a) Mean lateral error of the proposed methods based on number of received satellites using a commercial sensor. (b) Number of epochs based on number of received satellites a commercial sensor.

V. CONCLUSIONS

With the rise of multi-GNSS, more satellites are available, even in urban canyon environments. The possibility of using consistency check to detect and exclude faulty satellites, typically caused by multipath and NLOS, is therefore increasing. This study implements two multiple FDE methods and evaluates their performance in middle and deep urban canyons for application to vehicles with GPS, GLONASS, Beidou, and QZSS visibility. According to the experimental results, the FDE based on the greedy search method can greatly improve the positioning performance in middle urban canyons. Furthermore, the result of the greedy search is similar to that of the exhaustive search, which can be regarded as the theoretically best performance that FDE can achieve. Both greedy and exhaustive searches achieve sub-metre accuracy in terms of the mean lateral positioning error. For the case of deep urban canyons, both FDEs obtain only slight improvement and the lateral error can be more than 10 metres. As shown in the case study, there are more signals with visible LOS paths (LOS + Multipath) than not (NLOS). However, the strong multipath effects still result in both FDEs finding a consistent but erroneous group of satellites. Finally, we conclude that it is very difficult to obtain a lane-level positioning performance using only single frequency pseudorange level positioning in deep or dense urban environments.

REFERENCES

[1] S. Kamijo, Y. Gu, and L.-T. Hsu, "Autonomous Vehicle Technologies: Localization and Mapping," *IEICE Fundamentals Review,* vol. 9, pp. 131-141, October, 2015 2015.

[2] Y. Gu, L.-T. Hsu, and S. Kamijo, "Passive Sensor Integration for Vehicle Self-Localization in Urban Traffic Environment," *Sensors,* vol. 15, p. 29795, 2015.

[3] P. Misra and P. Enge, *Global Positioning System: Signals, Measurements, and Performance*. Lincoln, MA 01773 Ganga-Jamuna Press, 2011.

[4] S. Zhao, X. Cui, F. Guan, and M. Lu, "A Kalman Filter-Based Short Baseline RTK Algorithm for Single-Frequency Combination of GPS and BDS," *Sensors,* vol. 14, p. 15415, 2014.

[5] S.-S. Jan and S.-C. Lu, "Implementation and Evaluation of the WADGPS System in the Taipei Flight Information Region," *Sensors,* vol. 10, p. 2995, 2010.

[6] M. G. Petovello and P. D. Groves, "Multipath vs. NLOS signals," *Inside GNSS,* vol. 8, pp. 40-42, 2013.

[7] N. G. Ferrara, J. Nurmi, and E. S. Lohan, "Multi-GNSS analysis based on full constellations simulated data," in *2016 International Conference on Localization and GNSS (ICL-GNSS)*, 2016, pp. 1-6.

[8] A. Yasuda, "Multi-GNSS Demonstration Campaign in Asia Oceania Region," presented at the United Nations International Meeting on the Applications of Global Navigation Satellite Systems, Vienna, Austria, 2011.

[9] P. D. Groves, *Principles of GNSS, Inertial, and Multi-Sensor Integrated Navigation Systems (GNSS Technology and Applications)*, 2nd ed.: Artech House Publishers, 2013.

[10] M. S. Braasch, "Multipath Effects," in *Global Positioning System: Theory and Applications*. vol. 1, B. W. Parkinson and J. J. Spilker, Eds., ed Washington, DC: AIAA, 1996, pp. 547-568.

[11] A. J. V. Dierendonck, P. Fenton, and T. Ford, "Theory and Performance of Narrow Correlator Spacing in GPS Receiver," *NAVIGATION, Journal of The Institute of Navigation,* vol. 39, pp. 265-283, Fall 1992.

[12] L. Garin, F. v. Diggelen, and J.-M. Rousseau, "Strobe & Edge Correlator Multipath Mitigation for Code," in *Proceedings of the 9th International Technical Meeting of the Satellite Division of The Institute of Navigation (ION GPS 1996)*, Kansas City, MO, 1996, pp. 657-664.

[13] D. J. Jwo and S. H. Wang, "Adaptive Fuzzy Strong Tracking Extended Kalman Filtering for GPS Navigation," *IEEE Sensors Journal,* vol. 7, pp. 778-789, 2007.

[14] L.-T. Hsu, S.-S. Jan, P. Groves, and N. Kubo, "Multipath mitigation and NLOS detection using vector tracking in urban environments," *GPS Solutions,* vol. 19, pp. 249-262, April 2015.

[15] M. Lashley and D. M. Bevly. (2009) What are vector tracking loops, and what are their benefits and drawbacks? *Inside GNSS*. 16-21. Available: http://www.insidegnss.com/auto/mayjune09-gnss-sol.pdf

[16] M. Zhong, J. Guo, and Q. Cao, "On Designing PMI Kalman Filter for INS/GPS Integrated Systems With Unknown Sensor Errors," *IEEE Sensors Journal,* vol. 15, pp. 535-544, 2015.

[17] M. A. K. Jaradat and M. F. Abdel-Hafez, "Enhanced, Delay Dependent, Intelligent Fusion for INS/GPS Navigation System," *IEEE Sensors Journal,* vol. 14, pp. 1545-1554, 2014.

[18] C.-H. Tseng, S.-F. Lin, and D.-J. Jwo, "Fuzzy Adaptive Cubature Kalman Filter for Integrated Navigation Systems," *Sensors,* vol. 16, p. 1167, 2016.

[19] M. Rabbou and A. El-Rabbany, "Integration of GPS Precise Point Positioning and MEMS-Based INS Using Unscented Particle Filter," *Sensors,* vol. 15, p. 7228, 2015.

[20] K.-W. Chiang, T. Duong, and J.-K. Liao, "The Performance Analysis of a Real-Time Integrated INS/GPS Vehicle Navigation System with Abnormal GPS Measurement Elimination," *Sensors,* vol. 13, pp. 10599-10622, 2013.

[21] W. Jiang, Y. Li, and C. Rizos, "Optimal Data Fusion Algorithm for Navigation Using Triple Integration of PPP-GNSS, INS, and Terrestrial Ranging System," *IEEE Sensors Journal,* vol. 15, pp. 5634-5644, 2015.

[22] G. Kletetschka, J. Vyhnanek, D. Kawasumiova, L. Nabelek, and V. Petrucha, "Localization of the Chelyabinsk Meteorite From Magnetic Field Survey and GPS Data," *IEEE Sensors Journal,* vol. 15, pp. 4875-4881, 2015.

[23] Z. Hemin, Y. Weizheng, S. Qiang, L. Tai, and C. Honglong, "A Handheld Inertial Pedestrian Navigation System With Accurate Step Modes and Device Poses Recognition," *Sensors Journal, IEEE,* vol. 15, pp. 1421-1429, 2015.

[24] L.-T. Hsu, Y. Gu, Y. Huang, and S. Kamijo, "Urban Pedestrian Navigation using Smartphone-based Dead Reckoning and 3D Maps Aided GNSS," *Sensors Journal, IEEE,* vol. 16, pp. 1281-1293, 2016.

[25] P. D. Groves, "Shadow Matching: A New GNSS Positioning Technique for Urban Canyons," *The Journal of Navigation,* vol. 64, pp. 417-430, 2011.

[26] K. A. B. Ahmad, M. Sahmoudi, C. Macabiau, A. Bourdeau, and G. Moura, "Reliable GNSS Positioning in Mixed LOS/NLOS Environments Using a 3D Model," in *European Navigation Conference (ENC)*, Vienne, Austria, 2013.

[27] L.-T. Hsu, Y. Gu, and S. Kamijo, "3D building model-based pedestrian positioning method using GPS/GLONASS/QZSS and its reliability calculation," *GPS Solutions,* vol. 20, pp. 413–428, 2015/03/28 2016.

[28] L. Wang, P. D. Groves, and M. K. Ziebart, "GNSS Shadow Matching: Improving Urban Positioning Accuracy Using a 3D City Model with Optimized Visibility Scoring Scheme," *NAVIGATION, Journal of The Institute of Navigation,* vol. 60, pp. 195-207, 2013.

[29] T. Suzuki, Y. Amano, T. Hashizume, and N. Kubo, "Vehicle Teleoperation Using 3D Maps and GPS Time Synchronization," *Computer Graphics and Applications, IEEE,* vol. 33, pp. 82-88, 2013.

[30] J. Meguro, T. Murata, J. Takiguchi, Y. Amano, and T. Hashizume, "GPS Multipath Mitigation for Urban Area Using Omnidirectional Infrared Camera," *Intelligent Transportation Systems, IEEE Transactions on,* vol. 10, pp. 22-30, 2009.

[31] P. D. Groves and Z. Jiang, "Height Aiding, C/N 0 Weighting and Consistency Checking for GNSS

NLOS and Multipath Mitigation in Urban Areas," *The Journal of Navigation,* vol. 66, pp. 653-669, 2013.

[32] R. G. Brown, "A BASELINE GPS RAIM SCHEME AND A NOTE ON THE EQUIVALENCE OF THREE RAIM METHODS," *NAVIGATION, Journal of The Institute of Navigation,* vol. 39, pp. 301-316., Fall 1992.

[33] B. S. Pervan, S. P. Pullen, and J. R. Christie, "A MULTIPLE HYPOTHESIS APPROACH TO SATELLITE NAVIGATION INTEGRITY," *NAVIGATION, Journal of The Institute of Navigation,* vol. 45, pp. 61-84, 1998.

[34] T. Walter and P. Enge, "Weighted RAIM for Precision Approach," in *Proceedings of the 8th International Technical Meeting of the Satellite Division of The Institute of Navigation (ION GPS 1995)*, Palm Springs, CA, USA, 1995, pp. 1995-2004.

[35] T. Iwase, N. Suzuki, and Y. Watanabe, "Estimation and exclusion of multipath range error for robust positioning," *GPS Solutions,* vol. 17, pp. 53-62, January 2013.

[36] J. Blanch, T. Walter, and P. Enge, "Efficient Multiple Fault Exclusion with a Large Number of Pseudorange Measurements," in *Proceedings of the 2015 International Technical Meeting of The Institute of Navigation*, Dana Point, California, 2015.

[37] H. Tokura, H. Yamada, N. Kubo, and S. Pullen, "Using Multiple GNSS Constellations with Strict Quality Constraints for More Accurate Positioning in Urban Environments," *Positioning,* vol. 5, pp. 85-96, 2014.

[38] E. J. Candes and M. B. Wakin, "An Introduction To Compressive Sampling," *Signal Processing Magazine, IEEE,* vol. 25, pp. 21-30, 2008.

[39] M. Elad, *Sparse and Redundant Representations: From Theory to Applications in Signal and Image Processing*, 1 ed.: Springer-Verlag New York, 2010.

[40] H. Hartinger and F. K. Brunner, "Variances of GPS Phase Observations: The SIGMA-ε Model," *GPS Solutions,* vol. 2, pp. 35-43, April 1999.

[41] J. Blanch, T. Walter, P. Enge, S. Wallner, F. A. Fernandez, R. Dellago*, et al.*, "Critical Elements for a Multi-Constellation Advanced RAIM," *NAVIGATION, Journal of the Institute of Navigation,* vol. 60, pp. 53-69, Spring 2013.